BJR https://doi.org/10.1259/bjr.20201249

Received: 19 October 2020 | Revised: 13 January 2021 | Accepted: 14 January 2021

Cite this article as:
Orii M, Sugawara T, Takagi H, Nakano S, Ueda H, Takizawa Y, et al. Reliability of respiratory-triggered two-dimensional cine k-adaptive-t-autocalibrating reconstruction for Cartesian sampling for the assessment of biventricular volume and function in patients with repaired tetralogy of Fallot. *Br J Radiol* 2021; **94**: 20201249.

FULL PAPER

Reliability of respiratory-triggered two-dimensional cine k-adaptive-t-autocalibrating reconstruction for Cartesian sampling for the assessment of biventricular volume and function in patients with repaired tetralogy of Fallot

[1]MAKOTO ORII, MD, PhD, [2]TSUYOSHI SUGAWARA, RT, [1,3]HIDENOBU TAKAGI, MD, PhD, [4]SATOSHI NAKANO, MD, PhD, [5]HIRONOBU UEDA, MD, [4]YURIE TAKIZAWA, MD, PhD, [5]JUMPEI FUJIWARA, MD, [4]SHIN TAKAHASHI, MD, PhD, [4]KOTARO OYAMA, MD, PhD, [6,7]PENG LAI, PhD, [8]MARTIN A JANICH, PhD, [9]ATSUSHI NOZAKI and [1]KUNIHIRO YOSHIOKA, MD, PhD

[1]Department of Radiology, Iwate Medical University, Iwate, Japan
[2]Department of Radiology Service, Iwate Medical University, Iwate, Japan
[3]Department of Radiology, The University of British Columbia, St. Paul's Hospital, BC, Canada
[4]Department of Pediatrics, Iwate Medical University, Iwate, Japan
[5]Division of Cardiology, Department of Internal Medicine, Iwate Medical University, Iwate, Japan
[6]MR Applications and Workflow, GE Healthcare, Menlo Park, CA, USA
[7]Danaher Digital, San Jose, CA, USA
[8]MR Applications and Workflow, GE Healthcare, Munich, Germany
[9]MR Applications and Workflow, GE Healthcare, Tokyo, Japan

Address correspondence to: Dr Makoto Orii
E-mail: *kori931@gmail.com*

Objective: To compare left ventricular (LV) and right ventricular (RV) volume, function, and image quality of a respiratory-triggered two-dimensional (2D)-cine k-adaptive-t-autocalibrating reconstruction for Cartesian sampling (2D kat-ARC) with those of the standard reference, namely, breath-hold 2D balanced steady-state free precession (2D SSFP), in patients with repaired tetralogy of Fallot (TOF).
Methods: 30 patients (14 males, mean age 32.2 ± 13.9 years) underwent cardiac magnetic resonance, and 2D kat-ARC and 2D SSFP images were acquired on short-axis view. Biventricular end-diastolic volume (EDV) and end-systolic volume (ESV), stroke volume (SV), ejection fraction (EF), and LV mass (LVM) were analysed.
Results: The 2D kat-ARC had significantly shorter scan time (35.2 ± 9.1 s *vs* 80.4 ± 16.7 s; $p < 0.0001$). Despite an analysis of image quality showed significant impairment using 2D kat-ARC compared to 2D SSFP cine ($p < 0.0001$), the two sequences demonstrated no significant difference in terms of biventricular EDV, LVESV, LVSV, LVEF, and LVM. However, the RVESV was overestimated for 2D kat-ARC compared with that for 2D SSFP (73.8 ± 43.2 ml *vs* 70.3 ± 44.5 ml, $p = 0.0002$) and the RVSV and RVEF were underestimated (RVSV = 46.2±20.5 ml *vs* 49.4 ± 20.4 ml, $p = 0.0024$; RVEF = 40.2±12.7% vs. 43.5±14.0%, $p = 0.0002$).
Conclusion: Respiratory-triggered 2D kat-ARC cine is a reliable technique that could be used in the evaluation of LV volumes and function.
Advances in knowledge: 2D cine kat-ARC is a reliable technique for the assessment LV volume and function in patients with repaired TOF.

INTRODUCTION

Innovation in the management of tetralogy of Fallot (TOF) has led to dramatic improvements in early survival, but most patients suffer from pulmonary regurgitation (PR) and pulmonary stenosis (PS) after the operation.[1–3] These residual can induce biventricular dilatation, ventricular tachycardia (VT), and even sudden death,[4] but pulmonary valve replacement (PVR) can reduce the incidence of VT and possibly sudden death.[5–7] Recent guideline have described indications for PVR in TOF, which are based on biventricular ejection fraction (EF), right ventricular end-diastolic volume (RVEDV), RV end-systolic volume (RVESV), and exercise capacity.[8]

Cardiac magnetic resonance (CMR) represents a reliable technique for the evaluation of cardiac morphology, biventricular volumes, and systolic function.[9] Most commonly, biventricular volumes and EF are calculated by acquiring multiple and contiguous two-dimensional (2D) balanced steady-state free precession (SSFP) slices during breath-holds through the ventricles on short axis views.[10] However, 2D breath-hold cine SSFP (2D SSFP) sequences require several heartbeats' worth of breath holding for each slice. Therefore, this approach can be time-consuming and difficult in patients who are unable to hold their breath. Also, the inconsistent breath-hold position during the multiple breath-hold acquisition may cause misalignment of consecutive slices.[11,12] Recently, k-adaptive-t autocalibrating reconstruction for cartesian sampling (kat-ARC) was investigated for 3D cine to overcome the technical limitations of 2D SSFP.[13–16] This sequence directly synthesises unsampled data in k-t space, utilising spatial and temporal correlations with the temporal window in the k-t synthesis kernel selected per cardiac phase based on local cardiac motion to minimise motion blurring. However, no data are available concerning the reliability of respiratory-triggered 2D cine kat-ARC (2D kat-ARC) in clinical practice.

This study aimed to assess the image quality, reproducibility, and accuracy of 2D kat-ARC for the quantification of biventricular volumes and function in patients with repaired TOF.

METHODS AND MATERIALS

Study population and design

Between December 2018 and October 2019, 30 patients (14 [47%] males, mean age 32.2 ± 13.9 years) with repaired TOF at Iwate Medical University Hospital were prospectively recruited. Patients with supraventricular arrhythmias, non-MR compatible devices, or an inability to sustain a breath-hold were excluded from the study. The study protocol conforms to the ethical guidelines of the 1975 Declaration of Helsinki as reflected in an *a priori* approval by the institution's human research committee (MH2018-561), and written informed consent for data collection was obtained from each patient prior to the CMR.

CMR acquisition

All examinations were performed at 1.5 T (SIGNA Artist, GE Healthcare, Waukesha, WI) with a 33-channel phased array receiver coil. We initially recorded localising scans for determining ventricular long-axis orientation. Short-axis stack cine images were performed, in random order, in each patient using two different imaging techniques: the conventional 2D SSFP and 2D kat-ARC cine imaging. The basal most short-axis slice was located immediately on the myocardial side of the atrioventricular junction at the end-diastole prescribed from the previously acquired localising scans. The 2D SSFP cine was performed with multiple breath-holds with the following parameters: FOV = 360 × 360 mm, repetition time = 3.7 ms, echo time = 1.6 msec, flip angle = 60°, image matrix = 224×160, bandwidth = 892.9 Hz/pixel, slice thickness = 8 mm with a 2 mm gap, voxel size = 1.6 × 2.2 mm , and an acceleration factor of 2 using ASSET parallel imaging. The 2D kat-ARC was performed with free breathing with FOV = 360 × 360 mm, repetition time = 2.9 msec, echo time = 1.0 msec, flip angle = 60°, image matrix = 160×150, bandwidth = 1562.5 Hz/pixel, slice thickness = 8 mm with a with a 2 mm gap, voxel size = 2.2 × 2.4 mm , and an acceleration factor of 6 using kat-ARC. To reduce the breathing effects in image quality and volume quantification, the kat-ARC sequence was respiratory-triggered based on bellow signal with only ~50% data near end-expiration accepted for image reconstruction, and all data were acquired within a single heart beat for each slice (real-time acquisition). For 2D SSFP cine, a views/segment of 16 according the heart rate was used, resulting in a temporal resolution of 47 ms. The 2D kat-ARC sequence automatically adapts views/segment based on patient heart rate at scan time to collect 30 cardiac phases in a cardiac cycle. Both sequences were acquired with retrospective cardiac gating, and the acquired cardiac phases were linearly interpolated to 20 phases in 2D SSFP cine and 30 phases in 2D kat-ARC in a cardiac cycle.

Image analysis

The data sets of the cine images were transferred to an offline workstation, processed using commercially available software (Ziostation2, Ziosoft Inc., Tokyo, Japan) and evaluated by two expert readers with 8 and 7 years of experience in CMR performance and analysis, respectively. To estimate interobserver variability, each operator performed a blinded analysis on randomly rearranged sequences of all patients and one of the two observers repeated the analysis on all patients after at least 1 month.

The image quality scores were based on three main criteria: blood-to-myocardial contrast, endocardial edge delineation, and presence of motion artefacts throughout the cardiac cycle. The details of the image quality criteria are described elsewhere.[17] Each criterion was graded on a scale of 1 to 5, where 1 was non-diagnostic, 2 was suboptimal but still diagnostic for volumetric analysis, 3 was adequate, 4 was good, and 5 was excellent.

The endocardial and epicardial contours were automatically traced at end-systole and end-diastole with manual trace when required. The most basal section was defined as the section in which at least 50% of the border of the lumen was surrounded by myocardium. The papillary muscles and trabeculations of the RV were included as part of the blood pool.[18] The RV outflow tract was included as part of the RV blood volume. Subsequently, left ventricular end-diastolic volume (LVEDV), LV end-systolic volume (LVESV), LV stroke volume (LVSV), LVEF, as well as RVEDV, RVESV, RV stroke volume (RVSV), and RVEF were calculated by automatically tracing the endocardial contours on short-axis stacks in end-diastole and end-systole for both data set of sequences according to the Society for Cardiovascular Magnetic Resonance guidelines.[19] The LV mass (LVM) was calculated as the difference between the total epicardial volume and the total endocardial volume. The time required for imaging acquisition without gaps was recorded for both 2D SSFP cine and 2D kat-ARC.

Statistical analysis

All statistical analyses were performed using JMP® 13 (SAS Institute Inc., Cary, NC). Continuous variables are expressed as mean ± standard deviation (SD) or median and interquartile range as appropriate, whereas qualitative variables are expressed

Table 1. Baseline characteristics of the study population

Number of patients, n	30
Male/Female	14/16
Age, yrs	32.2 ± 13.9
Height, cm	156.6 ± 8.5
Weight, kg	57.9 ± 13.4
BSA, m^2	1.6 ± 0.2
Heart rate (beat/min)	69.9 ± 12.9
Respiration rate (breath/min)	20.4 ± 7.4

BSA, Body surface area.

as numbers and percentages. Normality was checked using the Shapiro-Wilk test. Differences between means were evaluated using paired and unpaired (for independent group comparisons) Student's *t*-tests for normally distributed data and Mann–Whitney or Wilcoxon signed rank tests for non-parametric data. The correlation between the parameters calculated from the 2D SSFP cine and 2D kat-ARC images were analysed using Pearson's correlation analysis. Bland–Altman analysis was performed to assess the interchangeability between the 2D SSFP cine and 2D kat-ARC image parameters, bias, and 95% limit of agreement, which was calculated by multiplying the SD by ±1.96. The inter- and intraobserver reproducibilities were assessed using intraclass correlation coefficients (ICCs) for absolute agreement of single measures with a 95% confidence interval (CI). Two-tailed $p < 0.05$ was considered statistically significant.

RESULTS

Population

The baseline characteristics of the study population are listed in Table 1. The 2D kat-ARC sequences were successfully performed and evaluated in all patients.

Intertechnique analysis

The time of acquisition without gaps of the 2D kat-ARC was significantly shorter than that of 2D SSFP (35.2 ± 9.1 s *vs* 80.4 ± 16.7 s, respectively; $p < 0.0001$) (Table 2). An analysis of image quality showed significant impairment of the 2D kat-ARC compared with the 2D SSFP with inferior results for blood-to-myocardial contrast, endocardial edge definition, and motion artefacts (Table 2).

The interobserver variability showed strong correlations for both sequences with the results of ICC (≥0.93) for all measurements of LV and RV (Table 3). The intraobserver differences were also strongly correlated, with ICC ≥0.95.

Correlations of the LV and RV functional parameters

The Bland–Altman plots showed strong agreement between the two sequences (Figures 1 and 2) and the linear regression yielded good agreement between the two techniques ($r \geq 0.92$) (Table 4).

Compared with 2D SSFP, 2D kat-ARC demonstrated no significant difference in terms of biventricular EDV, LVESV, LVSV, LVEF, and LVM. However, the RVESV for 2D kat-ARC was overestimated compared with that for 2D SSFP (2D kat-ARC = 73.8 ± 43.2 ml *vs* 2D SSFP = 70.3 ± 44.5 ml, respectively; $p = 0.0002$) (Table 5). The RVSV and RVEF for 2D kat-ARC were underestimated compared with those for 2D SSFP (2D kat-ARC RVSV = 46.2 ± 20.5 ml *vs* 2D SSFP = 49.4 ± 20.4 ml, $p = 0.0024$; 2D kat-ARC RVEF = 40.2 ± 12.7% vs. 2D SSFP = 43.5 ± 14.0%, $p = 0.0002$) (Table 5). A representative case is shown in Figures 3 and 4.

DISCUSSION

To the best of our knowledge, this study is the first to demonstrate the accuracy and reproducibility of the respiratory-triggered 2D cine using kat-ARC for the quantification of biventricular volumes and EF. The 2D kat-ARC has similar reproducibility to the conventional 2D SSFP sequence despite a reduction of image quality. Of note, the time of acquisition for 2D kat-ARC was significantly lower than that for 2D SSFP. The 2D kat-ARC sequences allow an accurate evaluation of LV volumes, LVEF, LVM, and RVEDV comparable to 2D SSFP sequences. However, the RVESV was overestimated and the RVSV and RVEF were underestimated for 2D kat-ARC compared with those for 2D SSFP in patients with repaired TOF.

The clinical course of repaired TOF patients is dependent on the degree of tricuspid regurgitation, PR, PS, and RV dilation, while long-term complications include aortic root dilation, LV dysfunction, and conduction and rhythm disturbances.[1–4] Hence, CMR parameters of RV size, function, and hypertrophy have been identified as predictors of death and VT in repaired TOF patients.[8,20] Therefore, CMR is invaluable for TOF imaging, especially post-operatively. 2D cine SSFP is the most common approach for the evaluation of volumes and systolic function in clinical practice. SSFP provides intrinsic advantages, especially its superior blood–myocardium contrast owing to blood in-flow effects. However, the conventional 2D cine SSFP sequence

Table 2. Comparison of image time of acquisition and quality between 2D SSFP and 2D kat-ARC

Parameter	2D SSFP	2D kat-ARC	*p*-value
Time of acquisition (s)	80.4 ± 16.7	35.2 ± 9.1	<0.0001
Blood-to-myocardial contrast	4.6 ± 0.8	3.7 ± 0.7	<0.0001
Endocardial edge definition	4.4 ± 0.8	3.5 ± 0.6	<0.0001
Motion artefact	4.4 ± 0.8	3.3 ± 0.5	<0.0001

2D SSFP, Two-dimensional steady-state free precession; 2D kat-ARC, Two-dimensional k-adaptive-t Autocalibrating Reconstruction for Cartesian sampling.

Table 3. (a) Interobserver variability of 2D SSFP and 2D kat-ARC of left ventricle. (b) Interobserver variability of 2D SSFP and 2D kat-ARC of right ventricle

(a)	2D SSFP (observer A)	2D SSFP (observer B)	ICC	CI 95% lower/upper	2D kat-ARC (observer A)	2D kat-ARC (observer B)	ICC	CI 95% lower/upper
LVEDV (ml)	75.2 ± 22.0	76.7 ± 20.9	0.988	0.969	74.4 ± 21.2	75.9 ± 20.7	0.981	0.957
				0.995				0.991
LVESV (ml)	38.6 ± 18.3	41.7 ± 18.8	0.981	0.571	38.8 ± 17.1	41.9 ± 16.9	0.981	0.120
				0.995				0.996
LVSV (ml)	36.6 ± 12.8	35.1 ± 11.6	0.951	0.892	35.6 ± 11.6	34.0 ± 11.6	0.945	0.875
				0.977				0.975
LVEF (%)	49.8 ± 12.4	47.0 ± 12.5	0.944	0.732	48.9 ± 11.7	45.5 ± 11.4	0.930	0.415
				0.980				0.980
LVM (g)	77.2 ± 21.8	74.5 ± 21.3	0.980	0.959	76.9 ± 21.3	74.9 ± 20.6	0.969	0.937
				0.990				0.985
(b)	2D SSFP (observer A)	2D SSFP (observer B)	ICC	CI 95%	2D kat-ARC (observer A)	2D kat-ARC (observer B)	ICC	CI 95%
RVEDV (ml)	119.7 ± 47.2	121.7 ± 49.1	0.990	0.979	120.0 ± 47.1	121.4 ± 49.3	0.992	0.982
				0.995				0.996
RVESV (ml)	70.3 ± 44.5	73.3 ± 44.7	0.994	0.973	73.8 ± 43.2	76.8 ± 42.9	0.996	0.927
				0.998				0.999
RVSV (ml)	50.0 ± 20.9	48.5 ± 18.0	0.955	0.909	46.2 ± 20.5	44.6 ± 20.0	0.955	0.909
				0.979				0.978
RVEF (%)	43.5 ± 14.0	42.1 ± 12.5	0.965	0.920	40.2 ± 12.7	38.0 ± 11.6	0.944	0.841
				0.984				0.977

2D SSFP, Two-dimensional steady state free precession; 2D kat-ARC, Two-dimensional k-adaptive-t Auto calibrating Reconstruction for Cartesian sampling; LVEDV, Left ventricular (LV) end-diastolic volume; LVEF, LV ejection fraction; LVESV, LV end-systolic volume; LVM, LV mass; LVSV, LV stroke volume; RVEDV, Right ventricular (RV) end-diastolic volume; RVEF, RV ejection fractionx Mark; RVESV, RV end-systolic volume; RVSV, RV stroke volume.

requires the suspension of respiration, and there are several factors that may limit the ability of patients to perform consistent breath-holds, such as anxiety, various medical conditions, and age.[11,12]

To overcome the technical limitations of 2D SSFP described above, several new cine sequences have been adopted to achieve faster CMR without affecting the temporal and spatial resolution of sequences.[11,21–24] In particular, compressed sensing-based approaches have been used to substantially accelerate 2D cine by exploring data sparsity along spatial and temporal dimensions. Additionally, kat-ARC has been developed for 3D cine imaging. Unlike other parallel imaging performed independently at each individual time frame, kat-ARC extends the data synthesis kernel along time to exploit both data correlation in k-space and temporal dimension with consequently improved reconstruction accuracy. Several studies have reported that the 3D cine kat-ARC is an accurate and reproducible technique for the evaluation of biventricular volumes and function in a single breath hold.[13–16] However, none of the studies have evaluated the performance of 2D cine with respiratory-triggered acquisition using kat-ARC.

Our study results showed good reproducibility of biventricular volume and EF between 2D SSFP and 2D kat-ARC sequences. Moreover, the 2D kat-ARC sequences allow an accurate evaluation of LV volumes, LVEF, LVM, and RVEDV compared with 2D SSFP. As a result of systolic motion of the mitral and tricuspid valve toward the apex (basal descent), care must be taken with the one or two most basal slices by using a consistent standardised approach.[25] A slice that contains LV and RV blood volume at end-diastole may include only left atrium (LA) and right atrium (RA) without ventricular blood volume at end-systole. The LA and RA can be identified by tracking wall thickening and cavity. Alternatively, the basal slice may be defined by at least 50% of the blood volume surrounded by myocardium. To reduce observer variability, we used the latter definition. Currently however, there is no expert consensus on which method to use. On the other hand, RVESV was overestimated

Figure 1. Bland–Altman parameters analysis results of left ventricle using 2D SSFP and 2D kat-ARC images. Caption: The graphs depict the relationships between the means and differences for each functional parameter. Solid line: bias; dotted lines: upper and lower 95% limits of agreement. 2D SSFP, Two-dimensional steady-state free precession; 2D kat-ARC, Two-dimensional k-adaptive-t autocalibratingreconstructionfor artesian sampling; LVEDV, Left ventricular (LV) end-diastolic volume; LVESV, LV end-systolic volume; LVSV, LV stroke volume; LVEF, LV ejection fraction; LVM, LV mass.

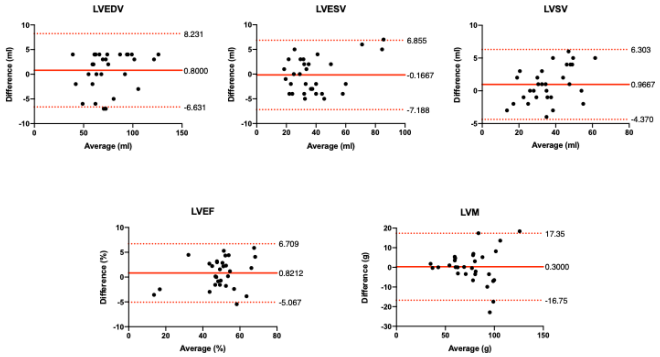

and RVSV and RVEF was underestimated for 2D kat-ARC compared with those for 2D SSFP. It has been reported that the tracing of endocardial contours on short-axis can be quite challenging in a dilated RV.[26] The RV in this study population was more dilated than the LV. Moreover, delineating the endocardium of the RV is more challenging than the LV owing to a greater proportion of trabeculated myocardium in patients with repaired TOF.[27] Tracing the RV boundary within the relatively thin compact myocardial layer may be preferable to an attempted tracing within the trabeculations. In contrast, hypertrophied trabeculations of the muscular part of the free wall may appear to merge in patients with repaired TOF, especially at end-systole. In this study, blood–myocardial boundaries were more blurred in the 2D kat-ARC sequence. Therefore, the boundary lines at end-systole might be located outside the trabecular layer, which would give a slightly larger end-systolic volume in the 2D kat-ARC sequence in this study. These results are consistent with a previous report comparing 2D SSFP and 4D flow kat-ARC.[16] The authors of that study concluded that a lower blood–myocardium contrast on the 4D flow kat-ARC images might be the reason for the overestimation of RVESV compared with 2D SSFP. Even though the difference in the values of RVESV and RVSV were within 5 ml, and RVEF was within 5% between two sequences, we should consider this technical limitation when tracing the RV boundary at end-systole in patients with repaired TOF.

Figure 2. Bland–Altman parameters analysis results of right ventricle using 2D SSFP and 2D kat-ARC images. Caption: The graphs depict the relationships between the means and differences for each functional parameter. Solid line: bias; dotted lines: upper and lower 95% limits of agreement. 2D SSFP, Two-dimensional steady-state free precession; 2D kat-ARC, Two-dimensional k-adaptive-t autocalibratingreconstructionfor artesian sampling; RVEDV, Right ventricular(RV) end-diastolic volume; RVESV, RV end-systolic volume; RVSV, RV stroke volume; RVEF, RV ejection fraction.

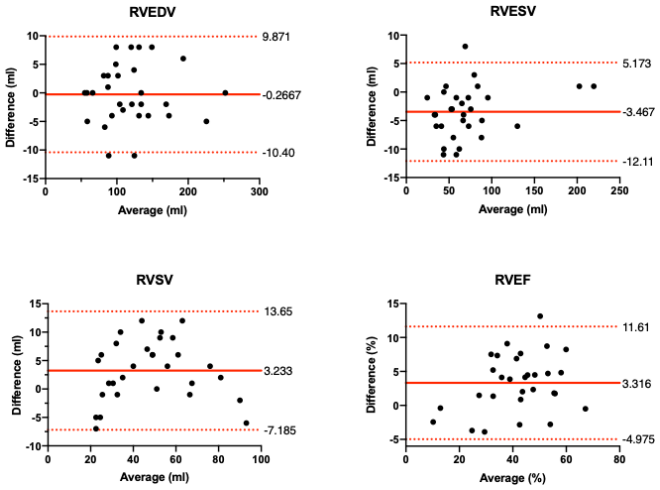

Table 4. Upper and lower 95% confidence interval between parameters calculated from 2D SSFP and 2D kat-ARC

			95% confidence interval	
	r value	*p*-value	Lower	Upper
LVEDV	0.9855	<0.0001	0.9693	0.9931
LVESV	0.9820	<0.0001	0.9620	0.9915
LVEF	0.9710	<0.0001	0.9293	0.9862
LVSV	0.9800	<0.0001	0.9679	0.9905
LVM	0.9201	<0.0001	0.8374	0.9616
RVEDV	0.9940	<0.0001	0.9873	0.9972
RVESV	0.9954	<0.0001	0.9901	0.9978
RVEF	0.9542	<0.0001	0.9050	0.9782
RVSV	0.9528	<0.0001	0.9023	0.9775

2D SSFP, Two-dimensional steady state free precession; 2D kat-ARC, Two-dimensional k-adaptive-t autocalibrating reconstruction for cartesian sampling; LVEDV, Left ventricular (LV) end-diastolic volume; LVEF, LV ejection fraction; LVESV, LV end-systolic volume; LVM, LV mass; LVSV, LV stroke volume; RVEDV, Right ventricular (RV) end-diastolic volume; RVEF, RV ejection fraction; RVESV, RV end-systolic volume; RVSV, RV stroke volume.

Several limitations of our study must be considered. First, we did not assess 2D SSFP and 2D kat-ARC sequences in healthy volunteers. In this study population, 10 of the 30 patients with repaired TOF had documented pulmonary hypertension on echocardiography performed no longer than 1 week prior to the MRI. The 2D SSFP images were obtained during an end-inspiratory breath-hold, which may affect the RV volume between the two sequences. Further studies are therefore needed to evaluate these sequences in normal control subjects. Second, we could not use the long-axis correction software for technical reasons. Further studies are needed in which the long-axis correction software can be used to make accurate measurements of the ventricular volume. Third, the most basal section was defined as the section in which at least 50% of the border of the lumen was surrounded by myocardium in this study. Although the 2D kat-ARC has similar reproducibility to the conventional 2D SSFP sequence

Table 5. Functional parameters of left and right ventricles and differences between 2D SSFP and 2D kat-ARC

Parameter	LVEDV (ml)	LVESV (ml)	LVSV (ml)	LVEF (%)	LVM (g)	RVEDV (ml)	RVESV (ml)	RVSV (ml)	RVEF (%)
2D SSFP	75.2 ± 22.1	38.6 ± 18.3	36.6 ± 12.8	49.8 ± 12.4	77.2 ± 21.8	119.7 ± 47.2	70.3 ± 44.5	49.4 ± 20.4	43.5 ± 14.0
2D kat-ARC	74.4 ± 21.2	38.8 ± 17.1	35.6 ± 11.6	48.9 ± 11.7	76.9 ± 21.3	120.0 ± 47.1	73.8 ± 43.2	46.2 ± 20.5	40.2 ± 12.7
2D SSFP - 2D kat-ARC	0.8 ± 3.8	−0.2 ± 3.6	1.0 ± 2.7	0.8 ± 3.0	0.3 ± 8.7	−0.3 ± 5.2	−3.5 ± 4.4	3.2 ± 5.3	3.3 ± 4.2
(2D SSFP - 2D kat-ARC) / 2D SSFP (%)	0.7 ± 5.8	−1.6 ± 9.9	1.2 ± 8.7	0.4 ± 8.6	0.4 ± 0.6	−0.5 ± 4.9	−7.3 ± 9.1	5.3 ± 14.2	5.9 ± 11.6
p-value	0.2572	0.7224	0.0616	0.1330	0.7684	0.8681	0.0002	0.0024	0.0002

2D SSFP, Two-dimensional steady state free precession; 2D kat-ARC, Two-dimensional k-adaptive-t autocalibrating reconstruction for cartesian sampling; LVEDV, Left ventricular (LV) end-diastolic volume; LVEF, LV ejection fraction; LVESV, LV end-systolic volume; LVM, LV mass; LVSV, LV stroke volume; RVEDV, Right ventricular (RV) end-diastolic volume; RVEF, RV ejection fraction; RVESV, RV end-systolic volume; RVSV, RV stroke volume.

Figure 3. A representative case of 2D SSFP and 2D kat-ARC imaging in the same patient (end-diastole). Caption: End-diastole with the apex located through basal slices. 2D SSFP, Two-dimensional steady-state free precession; 2D kat-ARC, Two-dimensional k-adaptive-t autocalibratingreconstruction-for artesian sampling.

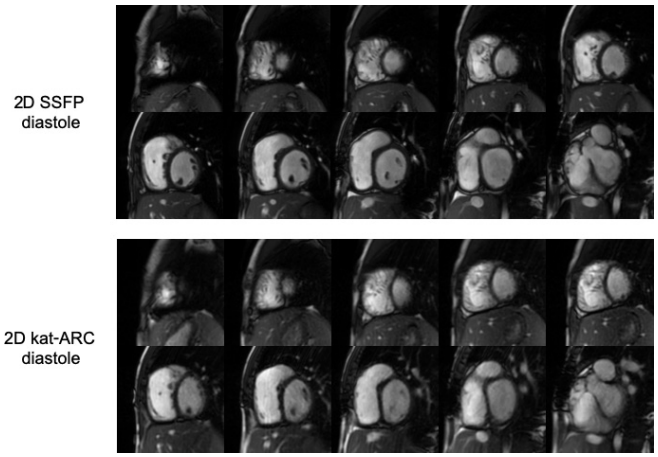

despite a reduction of image quality using this definition, we could not contour all the ventricular blood. Fourth, we did not evaluate regional myocardial wall motion and other morphologic abnormalities in both sequences. Finally, owing to the relatively small sample size, additional studies with a larger number of patients should be conducted to evaluate the robustness of the 2D kat-ARC technique.

CONCLUSION

This study demonstrates that respiratory-triggered 2D kat-ARC cine is a reliable and reproducible technique that could be used in the evaluation of biventricular volumes and function. However,

Figure 4. A representative case of 2D SSFP and 2D kat-ARC imaging in the same patient (end-systole). Caption: End-systole with the apex located through basal slices. There was substantial motion blurring and degradation of endocardial edge delineation with 2D kat-ARC cine imaging in end-systole. 2D SSFP, Two-dimensional steady-state free precession; 2D kat-ARC, Two-dimensional k-adaptive-t autocalibratingreconstructionfor artesian sampling.

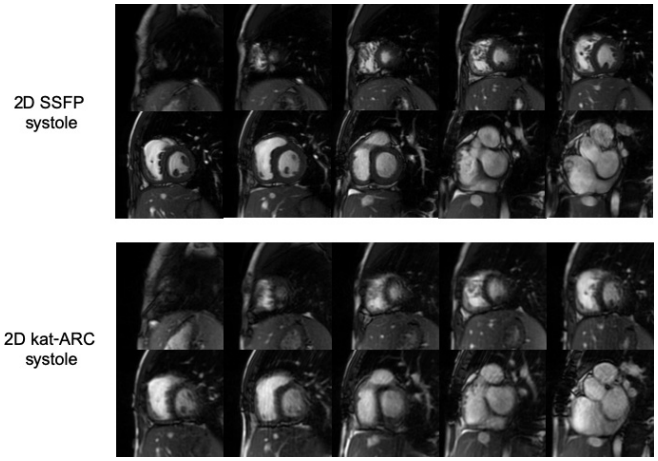

the RVESV was overestimated and the RVSV and RVEF were underestimated using 2D kat-ARC compared with those using conventional breath-hold 2D cine SSFP.

CONTRIBUTORS

MO designed and drafted the manuscript. MO and TS acquired data and performed measurements. SN, HU, YT, ST, and KO selected patients with repaired TOF. JF supported the statistical analysis. HT, PL, MJ, and AN supported the technical assistance. KY substantially contributed to the manuscript and revised itcritically for important intellectual content. All authors approved the submitted version.

ETHICS APPROVAL AND CONSENT TO PARTICIPATE

Informed written consent was obtained from all participants in this study. The study protocol was approved by the Ethics Committee of Iwate Medical University (MH2018-561) and the study has been performed in accordance with the Declaration of Helsinki.

AVAILABILITY OF DATA AND MATERIALS

The dataset analyzed during the current study are available from the corresponding author on reasonable request.

REFERENCES

1. Al Habib HF, Jacobs JP, Mavroudis C, Tchervenkov CI, O'Brien SM, Mohammadi S, et al. Contemporary patterns of management of tetralogy of Fallot: data from the Society of thoracic surgeons database. *Ann Thorac Surg* 2010; **90**: 813–20. doi: https://doi.org/10.1016/j.athoracsur.2010.03.110
2. Hickey EJ, Veldtman G, Bradley TJ, Gengsakul A, Manlhiot C, Williams WG, et al. Late risk of outcomes for adults with repaired tetralogy of Fallot from an inception cohort spanning four decades. *Eur J Cardiothorac Surg* 2009; **35**: 156–64. doi: https://doi.org/10.1016/j.ejcts.2008.06.050
3. Niwa K, Hamada H, Nakazawa M, Terai M, Tateno S, Sugimoto S, et al. Mortality and risk factors for late deaths in tetralogy of Fallot: the Japanese nationwide multicentric survey. *Cardiol Young* 2002; **12**: 453–60. doi: https://doi.org/10.1017/S104795110200077X
4. Gatzoulis MA, Balaji S, Webber SA, Siu SC, Hokanson JS, Poile C, et al. Risk factors for arrhythmia and sudden cardiac death late after repair of tetralogy of Fallot: a multicentre study. *Lancet* 2000; **356**: 975–81. doi: https://doi.org/10.1016/S0140-6736(00)02714-8
5. Geva T. Indications and timing of pulmonary valve replacement after tetralogy of Fallot repair. *Semin Thorac Cardiovasc Surg Pediatr Card Surg Annu* 2006; **9**: 11–22. doi: https://doi.org/10.1053/j.pcsu.2006.02.009
6. Therrien J, Provost Y, Merchant N, Williams W, Colman J, Webb G. Optimal timing for pulmonary valve replacement in adults after tetralogy of Fallot repair. *Am J Cardiol* 2005; **95**: 779–82. doi: https://doi.org/10.1016/j.amjcard.2004.11.037
7. Dos L, Dadashev A, Tanous D, Ferreira-González IJ, Haberer K, Siu SC, et al. Pulmonary valve replacement in repaired tetralogy of Fallot: determinants of early postoperative adverse outcomes. *J Thorac Cardiovasc Surg* 2009; **138**: 553–9. doi: https://doi.org/10.1016/j.jtcvs.2009.02.042
8. Stout KK, Daniels CJ, Aboulhosn JA, Bozkurt B, Broberg CS, Colman JM. AHA/ACC guideline for the management of adults with congenital heart disease: Executive summary: a report of the American College of Cardiology/American heart association Task force on clinical practice guidelines. *Circulation* 2018; **2019**: e637–97.
9. Carr JC, Simonetti O, Bundy J, Li D, Pereles S, Finn JP. Cine Mr angiography of the heart with segmented true fast imaging with steady-state precession. *Radiology* 2001; **219**: 828–34. doi: https://doi.org/10.1148/radiology.219.3.r01jn44828
10. Varga-Szemes A, Muscogiuri G, Schoepf UJ, Wichmann JL, Suranyi P, De Cecco CN, et al. Clinical feasibility of a myocardial signal intensity threshold-based semi-automated cardiac magnetic resonance segmentation method. *Eur Radiol* 2016; **26**: 1503–11. doi: https://doi.org/10.1007/s00330-015-3952-4
11. Goebel J, Nensa F, Schemuth HP, Maderwald S, Gratz M, Quick HH, et al. Compressed sensing cine imaging with high spatial or high temporal resolution for analysis of left ventricular function. *J Magn Reson Imaging* 2016; **44**: 366–74. doi: https://doi.org/10.1002/jmri.25162
12. Camargo GC, Erthal F, Sabioni L, Penna F, Strecker R, Schmidt M, et al. Real-Time cardiac magnetic resonance cine imaging with sparse sampling and iterative reconstruction for left-ventricular measures: comparison with gold-standard segmented steady-state free precession. *Magn Reson Imaging* 2017; **38**: 138–44. doi: https://doi.org/10.1016/j.mri.2017.01.002
13. Okuda S, Yamada Y, Tanimoto A, Fujita J, Sano M, Fukuda K, et al. Three-Dimensional cardiac cine imaging using the kat Arc acceleration: initial experience in clinical adult patients at 3T. *Magn Reson Imaging* 2015; **33**: 911–7. doi: https://doi.org/10.1016/j.mri.2015.04.004
14. Jeong D, Schiebler ML, Lai P, Wang K, Vigen KK, François CJ. Single breath hold 3D cardiac cine MRI using kat-ARC: preliminary results at 1.5T. *Int J Cardiovasc Imaging* 2015; **31**: 851–7. doi: https://doi.org/10.1007/s10554-015-0615-0
15. Muscogiuri G, Gatti M, Dell'Aversana S, Pica S, Andreini D, Guaricci AI, et al. Reliability of single breath hold three-dimensional cine kat-ARC for the assessment of biventricular dimensions and function. *Eur J Radiol* 2020; **124**: 108820. doi: https://doi.org/10.1016/j.ejrad.2020.108820
16. Vial J, Bouzerar R, Pichois R, Lhostis F, Raad O, Mathiron A, et al. Mri assessment of right ventricular volumes and function in patients with repaired tetralogy of Fallot using kat-ARC accelerated sequences. *AJR Am J Roentgenol* 2020; **215**: 807–17. doi: https://doi.org/10.2214/AJR.19.22726
17. Pednekar AS, Wang H, Flamm S, Cheong BY, Muthupillai R. Two-Center clinical validation and quantitative assessment of respiratory triggered retrospectively cardiac gated balanced-SSFP cine cardiovascular magnetic resonance imaging in adults. *J Cardiovasc Magn Reson* 2018; **20**: 44. doi: https://doi.org/10.1186/s12968-018-0467-6
18. Petersen SE, Aung N, Sanghvi MM, Zemrak F, Fung K, Paiva JM, et al. Reference ranges for cardiac structure and function using cardiovascular magnetic resonance (CMR) in Caucasians from the UK Biobank population cohort. *J Cardiovasc Magn Reson* 2017; **19**: 18. doi: https://doi.org/10.1186/s12968-017-0327-9
19. Kramer CM, Barkhausen J, Bucciarelli-Ducci C, Flamm SD, Kim RJ, Nagel E. Standardized cardiovascular magnetic resonance imaging

(CMR) protocols: 2020 update. *J Cardiovasc Magn Reson* 2020; **22**: 17. doi: https://doi.org/10.1186/s12968-020-00607-1

20. Muscogiuri G, Suranyi P, Eid M, Varga-Szemes A, Griffith L, Pontone G, et al. Pediatric cardiac MR imaging:: practical preoperative assessment. *Magn Reson Imaging Clin N Am* 2019; **27**: 243–62. doi: https://doi.org/10.1016/j.mric.2019.01.004
21. Jeong D, Schiebler ML, Lai P, Wang K, Vigen KK, François CJ. Single breath hold 3D cardiac cine MRI using kat-ARC: preliminary results at 1.5T. *Int J Cardiovasc Imaging* 2015; **31**: 851–7. doi: https://doi.org/10.1007/s10554-015-0615-0
22. Lin ACW, Strugnell W, Riley R, Schmitt B, Zenge M, Schmidt M, et al. Higher resolution cine imaging with compressed sensing for accelerated clinical left ventricular evaluation. *J Magn Reson Imaging* 2017; **45**: 1693–9. doi: https://doi.org/10.1002/jmri.25525
23. Rochitte CE, Azevedo CF, Rosário MA, Siqueira MHR, Monsão V, Saranathan M, et al. Single-breathhold four-dimensional assessment of left ventricular morphological and functional parameters by magnetic resonance imaging using the vast technique. *Open Cardiovasc Med J* 2011; **5**: 90–8. doi: https://doi.org/10.2174/1874192401105010090
24. Jaroni J, Meier R, Beer A, Herrmann K, Settles M, Rummeny EJ, et al. Three-Dimensional magnetic resonance imaging using single breath-hold k-t blast for assessment of global left ventricular functional parameters. *Acad Radiol* 2013; **20**: 987–94. doi: https://doi.org/10.1016/j.acra.2013.03.012
25. Schulz-Menger J, Bluemke DA, Bremerich J, Flamm SD, Fogel MA, Friedrich MG, et al. Standardized image interpretation and post-processing in cardiovascular magnetic resonance - 2020 update : Society for Cardiovascular Magnetic Resonance (SCMR): Board of Trustees Task Force on Standardized Post-Processing. *J Cardiovasc Magn Reson* 2020; **22**: 19. doi: https://doi.org/10.1186/s12968-020-00610-6
26. Bonnemains L, Mandry D, Marie P-Y, Micard E, Chen B, Vuissoz P-A. Assessment of right ventricle volumes and function by cardiac MRI: quantification of the regional and global interobserver variability. *Magn Reson Med* 2012; **67**: 1740–6. doi: https://doi.org/10.1002/mrm.23143
27. Kilner PJ, Geva T, Kaemmerer H, Trindade PT, Schwitter J, Webb GD. Recommendations for cardiovascular magnetic resonance in adults with congenital heart disease from the respective working groups of the European Society of cardiology. *Eur Heart J* 2010; **31**: 794–805. doi: https://doi.org/10.1093/eurheartj/ehp586